



PCCP

The charge/discharge mechanism and electrochemical performance of CuV₂O₆ as a new anode material for lithium ion batteries

| | |
|-------------------------------|--|
| Journal: | <i>Physical Chemistry Chemical Physics</i> |
| Manuscript ID: | CP-ART-06-2015-003435.R1 |
| Article Type: | Paper |
| Date Submitted by the Author: | 03-Jul-2015 |
| Complete List of Authors: | Ni, Shibing; three gorges university, College of Mechanical and Material Engineering Ma, Jianjun; Three gorges university, materials and chemical engineering Zhang, Jicheng; Three gorges university, materials and chemical engineering Yang, Xuelin; Three gorges university, materials and chemical engineering Zhang, Lulu; Three gorges university, materials and chemical engineering |
| | |

SCHOLARONE™
Manuscripts

Cite this: DOI: 10.1039/c0xx00000x

www.rsc.org/xxxxxx

ARTICLE TYPE

The charge/discharge mechanism and electrochemical performance of CuV_2O_6 as a new anode material for Li-ion batteries

Jianjun Ma,^a Shibing Ni,^{*a,b} Jicheng Zhang,^a Xuelin Yang^{*a,b}, and Lulu Zhang^{a,b}

Received (in XXX, XXX) Xth XXXXXXXXX 201X, Accepted Xth XXXXXXXXX 201X

DOI: 10.1039/b000000x

The charge/discharge mechanism of CuV_2O_6 as anode for Li-ion batteries is firstly studied, suggesting a phase transition in discharging, which involves the initial formation of LiV_2O_5 and $\text{Cu}_3\text{V}_2\text{O}_8$, the subsequent transition from $\text{Cu}_3\text{V}_2\text{O}_8$ to $\text{Li}_x\text{V}_2\text{O}_5$ and CuO , the insertion of lithium ions into LiV_2O_5 , and the later reduction of CuO into Cu . The phase transition of $\text{Cu}_3\text{V}_2\text{O}_8$ accompanies by an amorphization process, which maintains in the subsequent discharging and charging process. CuV_2O_6 /natural graphite electrode with sodium alginate binder is prepared, which shows superior electrochemical performance. At a specific current of 110 mA g^{-1} , it delivers initial discharge and charge capacity of 725 and 453 mAh g^{-1} , respectively, maintaining of 537 and 533 mAh g^{-1} after 200 cycles.

The development of Li-ion batteries accompanies by the discovery and exploration of new electrode materials. For example, the successful application of LiCoO_2 and LiFePO_4 as cathode and $\text{Li}_4\text{Ti}_5\text{O}_{12}$ as anode has largely promoted the development of Li-ion batteries.¹⁻³ By now, significant progress of Li-ion batteries has been acquired, whereas the explorization of new electrode materials is still under way.

Vanadium is a typical metal element with multiform valence state, which can form a series of metal vanadium oxides ($\text{M}_x\text{V}_y\text{O}_z$, $\text{M}=\text{Fe}, \text{Cu}, \text{Zn}, \text{Ag}, \text{Co}$ etc.) via combining with other metal element and oxygen element,⁴⁻⁸ demonstrating great potential as anode and/or cathode for Li-ion batteries. Among them, CuV_2O_6 was considered as a cathode material owing to its relative high voltage plateaus ($>2 \text{ V}$ versus Li metal).⁹⁻¹¹ For cathode, the excessive lithiation of CuV_2O_6 under lower voltage plateau is not favorable. On the one hand, it may result in irreversible phase transition owing to the structure destruction of CuV_2O_6 . On the other hand, the low voltage plateau is not beneficial to improve the energy density of Li-ion batteries when matching with an anode material. In contrast, the charge/discharge mechanism of CuV_2O_6 under lower voltage is of great interesting, which may endow it with potential application as anode for Li-ion batteries. However, no research on studying the electrochemical performance of CuV_2O_6 as anode for Li-ion batteries is reported by now.

Here in this paper, we aim to study the charge/discharge

mechanism and the electrochemical performance of CuV_2O_6 as anode for Li-ion batteries. During electrode preparation, low cost natural graphite (NG) and water soluble sodium alginate were adopted as conducting agent and binder, which are beneficial for large scale preparation. As results, the $\text{CuV}_2\text{O}_6/\text{NG}$ electrode shows superior electrochemical performance, demonstrating great potential of CuV_2O_6 as anode for Li-ion batteries.

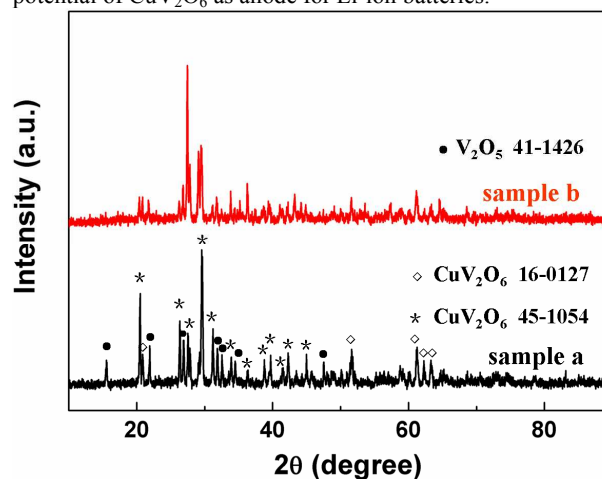


Fig. 1 XRD patterns of sample a and b.

XRD patterns of sample a and b are shown in Fig. 1. As seen, diffraction peaks located at 20.6° , 26.6° , 27.6° , 29.4° , 31.6° , 33.7° , 36.7° , 38.6° , 39.6° , 41.5° , 42.2° , and 44.8° can be attributed to the (200), (1-10), (110), (201), (1-11), (111), (11-2), (3-1-1), (3-10), (310), (20-3) and (003) faces of anorthic CuV_2O_6 (JCPDS, no. 45-1054). Meanwhile, diffraction peaks at 20.8° , 51.8° , 61.1° , 62.2° and 63.5° originate from other phase of CuV_2O_6 (JCPDS, no. 16-0127). The diffraction peaks locate at 15.3° , 21.7° , 26.2° , 31.0° , 32.4° , 34.3° and 47.3° correspond to the (200), (101), (110), (400), (011), (310) and (600) faces of orthorhombic V_2O_5 (JCPDS, no. 41-1426). Tuning the mole ratio between precursor $\text{CuSO}_4 \cdot 5\text{H}_2\text{O}$ and V_2O_5 is not a guarantee to obtain pure CuV_2O_6 , whereas the oriented growth of CuV_2O_6 can be affected.

Fig. 2(a) is a low magnification SEM image of sample a, which exhibits a large number of micro-particles with mean size about $1 \mu\text{m}$. A high magnification SEM image of sample a is shown in Fig. 2(b), which suggests these micro-particles are of smooth surface with sphere-like and block-like morphologies. The size of

these micro-spheres ranges from 500 nm to 1.5 μm , and the mean length, width and thickness of these micro-blocks are 1.5 μm , 600 nm and 400 nm, respectively. For further clarifying the morphology and microstructure of the CuV_2O_6 , TEM and HRTEM images were provided. As shown in a low magnification TEM image in Fig. 2(c), the CuV_2O_6 shows clear sphere-like and block-like morphologies, which are in accordance with those in SEM images. The inset of Fig. 2(c) is a SAED pattern of a single

CuV_2O_6 micro-block, which exhibit regular diffraction spots, suggesting the CuV_2O_6 is well crystallized. Fig. 2(d) is a HRTEM image of the sample, which shows clear lattice fringes. The interplanar spacing is 0.304 nm, which corresponds to the (201) face of anorthic CuV_2O_6 .

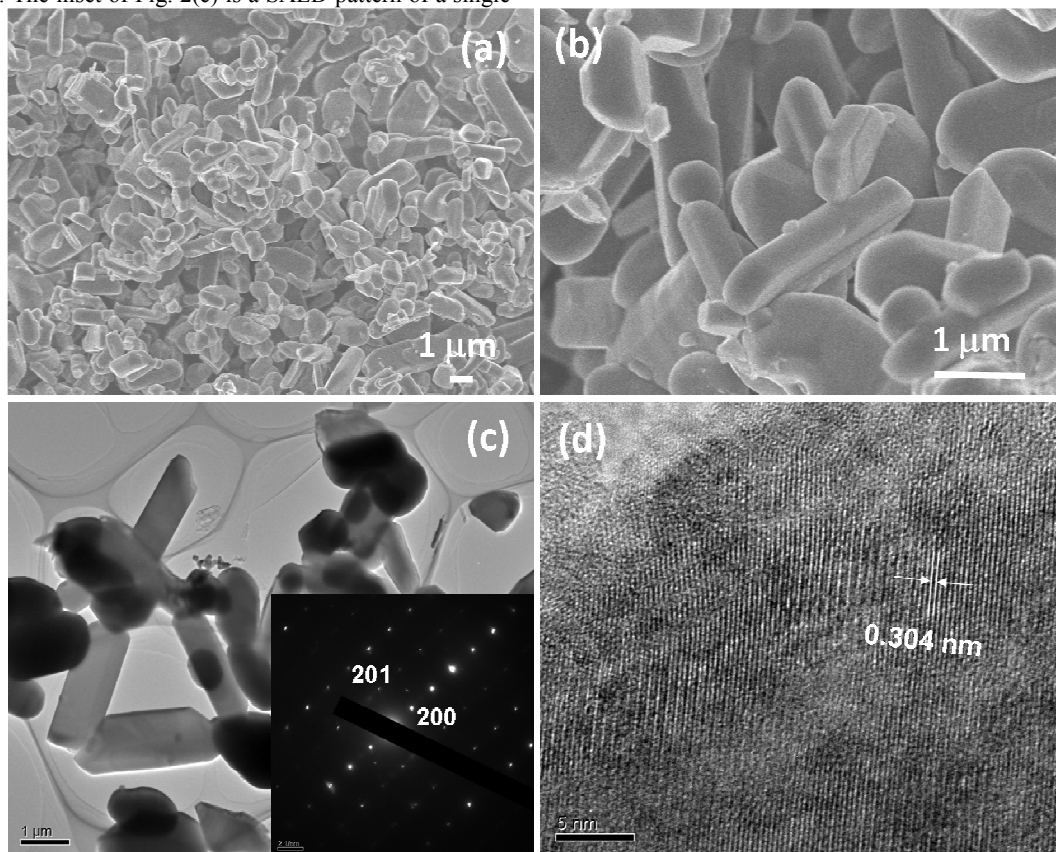


Fig. 2 SEM, TEM and HRTEM images of sample a. (a) low and (b) high magnification SEM image. (c) TEM and (d) HRTEM image. The inset of (c) is a SAED pattern.

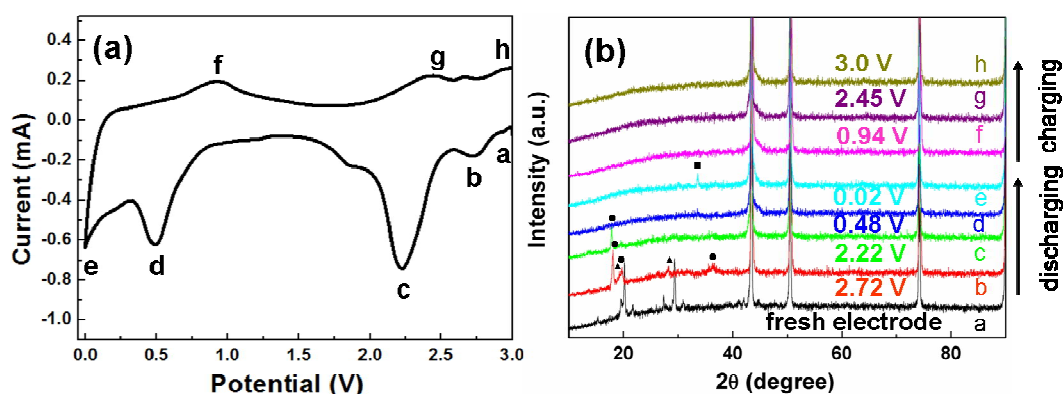


Fig. 3 (a) The initial CV curve of pristine CuV_2O_6 electrode. (b) XRD patterns of pristine CuV_2O_6 electrode under different discharge and charge states.

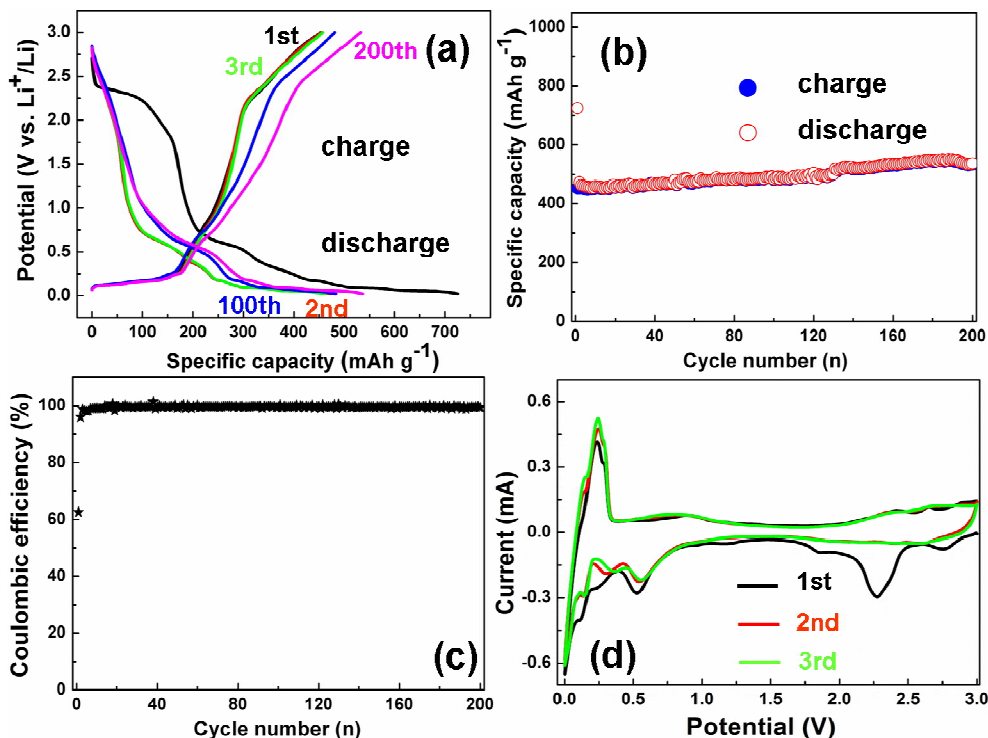


Fig. 4 Electrochemical performance of $\text{CuV}_2\text{O}_6/\text{NG}$ electrode (sample a). (a) The galvanostatic charge/discharge voltage profiles for the initial three, the 100th and 200th cycles. (b) Capacity retention of the galvanostatic test runs at a specific current of 110 mA g^{-1} . (c) Coulombic efficiency. (d) Cyclic voltammograms at a scan rate of 0.2 mV s^{-1} .

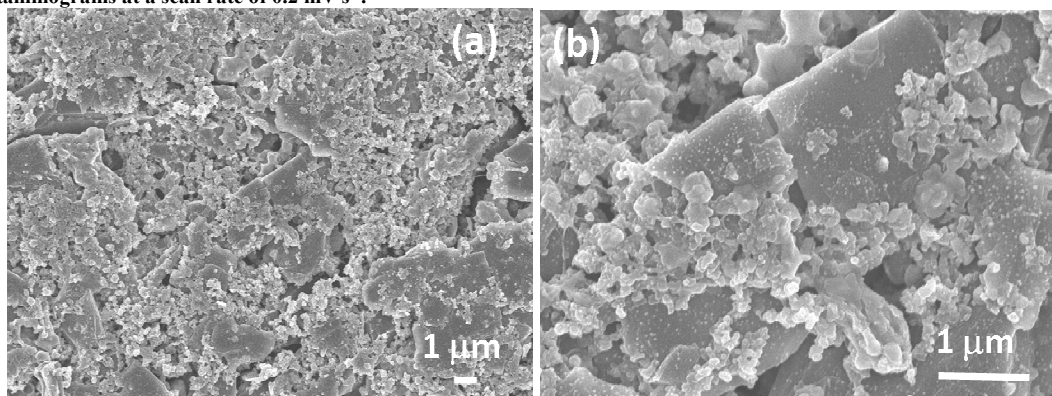


Fig. 5 SEM images of $\text{CuV}_2\text{O}_6/\text{NG}$ electrode (sample a) after cycling test with low (a) and high (b) magnification.

XRD patterns of pristine CuV_2O_6 electrode under different states in the initial cycle were studied to understand the electrochemical behavior of CuV_2O_6 in voltage region 3~0.02 V. The charge and discharge state was selected according to the initial CV curve as shown in Fig. 3(a). As seen, when discharging to 2.72 V, new diffraction peaks near 18.0° , 19.6° and 36.3° (marked by \bullet) appear, corresponding to the (010), (110) and (020) faces of $\delta\text{-LiV}_2\text{O}_5$ (JCPDS, no 34-1435). Meanwhile, a new diffraction peak near 19.2° and 28.3° (marked by \blacktriangle) can be attributed to the (010) and (-1-11) faces of orthorhombic $\text{Cu}_3\text{V}_2\text{O}_8$ (JCPDS, no 74-1401). The electrochemical reaction in this voltage region can be described as: $2\text{Li}^+ + 2\text{e}^- + 3\text{CuV}_2\text{O}_6 \rightarrow \text{Cu}_3\text{V}_2\text{O}_8 + 2\text{LiV}_2\text{O}_5$, which is similar to that of CoV_2O_6 .⁸ The diffraction peaks of $\text{Cu}_3\text{V}_2\text{O}_8$ disappear when further discharging to 2.22 V, corresponding to the phase transition from $\text{Cu}_3\text{V}_2\text{O}_8$ into amorphous $\text{Li}_x\text{V}_2\text{O}_5$ and CuO , which is similar to that of

$\text{Co}_3\text{V}_2\text{O}_8$.¹² Meanwhile, the diffraction peak of LiV_2O_5 shows little shift towards low 2θ degree, which suggests increased interplanar spacing owing to the insertion of lithium ions into LiV_2O_5 . The electrochemical reaction in this voltage region can be described as: $x\text{Li}^+ + x\text{e}^- + \text{Cu}_3\text{V}_2\text{O}_8 \rightarrow 3\text{CuO} + 2\text{Li}_x\text{V}_2\text{O}_5$ and $x\text{Li}^+ + x\text{e}^- + \text{LiV}_2\text{O}_5 \rightarrow \text{Li}_x\text{V}_2\text{O}_5$. In the subsequent discharging process, the diffraction peak of $\text{Li}_x\text{V}_2\text{O}_5$ disappears when further discharging to 0.48 V, suggesting the amorphization of $\text{Li}_x\text{V}_2\text{O}_5$ along with the increasing of x in $\text{Li}_x\text{V}_2\text{O}_5$. Electrochemical reactions in voltage region 2.22~0.48 V can be described as: $x\text{Li}^+ + x\text{e}^- + \text{LiV}_2\text{O}_5 \rightarrow \text{Li}_x\text{V}_2\text{O}_5$. Meanwhile, new diffraction peak near 33.6° (marked by \blacksquare) appears when discharging to 0.02 V, which corresponds to the (111) face of Li_2O . The electrochemical reaction in voltage region 0.48~0.02 V can be described as: $\text{CuO} + 2\text{Li}^+ + 2\text{e}^- \rightarrow \text{Cu} + \text{Li}_2\text{O}$. In the subsequent charging process, amorphous state of the electrode was preserved, corresponding to

the extraction of lithium ions from $\text{Li}_x\text{V}_2\text{O}_5$ and the oxidation of Cu into Cu_2O ,¹³ being similar to that of CoV_2O_6 .⁸

Galvanostatic charge/discharge cycling of the $\text{CuV}_2\text{O}_6/\text{NG}$ electrode (sample a) was carried out in the potential window of 3~0.02 V versus Li. Fig. 4(a) is the initial three, the 100th and 200th charge and discharge curves at a specific current of 110 mA g^{-1} . As seen, the initial discharge curve differs slightly from the subsequent ones, showing a potential plateau near 2.3 V and three sloping potential regions (1.9~0.74, 0.74~0.3 and 0.3~0.02 V) for multistep electrochemical reactions for the generation of LiV_2O_5 and $\text{Cu}_3\text{V}_2\text{O}_8$, the subsequent transition from $\text{Cu}_3\text{V}_2\text{O}_8$ to $\text{Li}_x\text{V}_2\text{O}_5$ and CuO, the reduction of CuO into Cu, as well as the insertion of lithium ions into NG.^{8,12,14} The potential plateau disappears in the subsequent discharge curves, which exhibit three sloping potential regions (1.9~0.7, 0.7~0.2 and 0.2~0.02 V), suggesting irreversible phase transition in the initial cycle. All the charge curves show similar profiles with three sloping potential regions (0.08~0.3, 0.3~2.2 and 2.2~3 V), which correspond to the extraction of lithium ions from NG and $\text{Li}_x\text{V}_2\text{O}_5$ as well as the oxidation of Cu into Cu_2O .^{8,12,14} As shown in Fig. 4(b), the initial discharge and charge capacity are 725 and 453 mAh g^{-1} , and the capacity loss is relevant to the irreversible phase transition. In the subsequent cycles, both the discharge and charge capacity increase slowly in the first few cycles owing to the activation of the electrode and then gradually reach stable values. After 200 cycles, the discharge and charge capacity maintain of 537 and 533 mAh g^{-1} , respectively. Corresponding coulombic efficiency (defined as $C_{\text{charge}}/C_{\text{discharge}}$) of the $\text{CuV}_2\text{O}_6/\text{NG}$ electrode is shown in Fig. 4(c). As seen, it exhibits a low initial coulombic efficiency of 62.5% owing to irreversible phase transition. In the subsequent cycles, the coulombic efficiency distinctly improves along with cycle number, showing a mean value of 99.3 % over 200 cycles, which suggests highly reversible lithiation and delithiation process. The cyclic voltammetric (CV) curves of the $\text{CuV}_2\text{O}_6/\text{NG}$ electrode was tested in voltage region 0~3.0 V at a scan rate of 0.2 mV s^{-1} . As shown in Fig. 4(d), the profiles of CV curves for the 2nd and 3rd cycle are similar, whereas an obvious difference between the first and subsequent two cycles is found. In the 1st cathodic scan, a strong reduction peak near 2.28 V and two weak reduction peaks near 1.86 and 2.76 V in high voltage region can ascribe to the phase transition from CuV_2O_6 to $\text{Li}_x\text{V}_2\text{O}_5$ and $\text{Cu}_3\text{V}_2\text{O}_8$.^{8,12} Three reduction peaks near 0.53, 0.23 and 0.12 V in the low voltage region can be attributed to the transition of $\text{Cu}_3\text{V}_2\text{O}_8$ into $\text{Li}_x\text{V}_2\text{O}_5$ and CuO, the reduction of CuO into Cu, as well as the insertion of lithium ions into NG, respectively.^{8,12,14} Meanwhile, the reduction peaks near 0.53 and 0.23 V shift to 0.56 and 0.3 V owing to the activation of the electrode. The reduction peak at 0.12 V shows no obvious variation, which suggests stable lithiation of NG in cycling. In the anodic scan, a strong oxidation peak near 0.24 V can be attributed to the extraction of lithium ions from NG,¹⁴ and a weak oxidation peak near 0.86 V can ascribe to the oxidation of Cu into Cu_2O .¹³ Meanwhile, a wide oxidation peak in the voltage region 2~3 V can ascribe to the extraction of lithium ions from $\text{Li}_x\text{V}_2\text{O}_5$.^{8,12} The electrochemical reactions during the discharge and charge process are similar to those of CoV_2O_6 .⁸

Fig. 5(a) is a low magnification SEM image of the $\text{CuV}_2\text{O}_6/\text{NG}$ electrode after 100 cycles with charge state, which exhibits an

integrated film-like morphology that consists of a large number of micro-flakes and nanoparticles, corresponding to NG and cycled CuV_2O_6 , respectively. For further clarifying the surface morphology of the cycled electrode, a high magnification SEM image of the cycled electrode is shown in Fig. 5(b). As seen, NG is well surrounded by a large number of particles with mean size about 100 nm. These particles don't tend to aggregate, assembling into new porous architecture in combination with NG. Meanwhile, smaller particles with mean size about several nanometers are observed, which locate on the surface of NG and bigger particles. The morphology of the cycled CuV_2O_6 differs much from that before cycling, which can be understood as an electrochemical reconstruction effect. Firstly, a large number of small particles form owing to a phase transition of CuV_2O_6 in discharging process, which can be describes as electrochemical activation.^{15,16} However, the aggregation of these small particles are prevented owing to the separating effect of flaky NG, assembling into porous architecture in combination with NG in the subsequent process, which can be described as electrochemical reconstruction.^{17,18} In the reconstructed electrode, the porous architecture is beneficial for the contact between electrode and electrolyte, and the small size of the cycled CuV_2O_6 and the good contact between the cycled CuV_2O_6 and NG can provide high Li-ion storage performance and high electronic conductivity, respectively. As results, the $\text{CuV}_2\text{O}_6/\text{NG}$ electrode exhibits superior electrochemical performance.

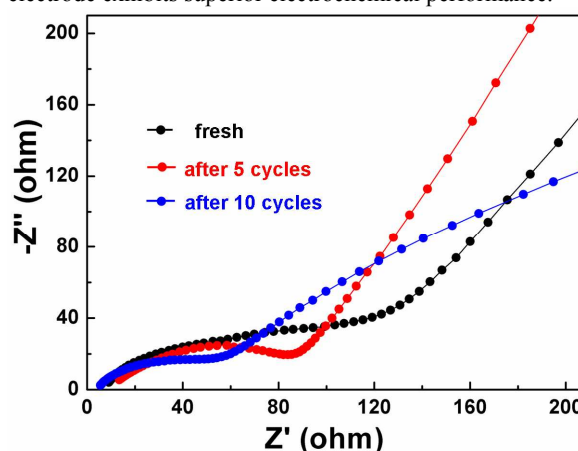


Fig. 6 EIS spectra of $\text{CuV}_2\text{O}_6/\text{NG}$ electrode (sample a) with different states.

Fig. 6 shows the EIS spectra of the $\text{CuV}_2\text{O}_6/\text{NG}$ electrode (sample a) with different states. For fresh electrode, the intercept in high-frequency can be attributed to the ohmic resistance caused by the electrolyte (R_s), the medium-frequency semicircle is due to the charge-transfer resistance on electrode/electrolyte interface (R_{ct}), and the inclined line in low-frequency corresponds to the lithium ion diffusion process within electrode.¹⁹ For the cycled electrode, the intercept in high-frequency mainly originates from SEI film resistance (R_e), the medium-frequency semicircle corresponds to the charge-transfer impedance on electrode/electrolyte interface (R_{ct}), and the inclined line in low-frequency corresponds to the lithium ion diffusion process within electrode.²⁰ The fresh and cycled electrodes were fitted by $R(C(RW))$ equivalent circuit, and the fitted results are shown in Tab. 1. As seen, R_e increases firstly and then decreases in cycling, which may be relevant to the gradual

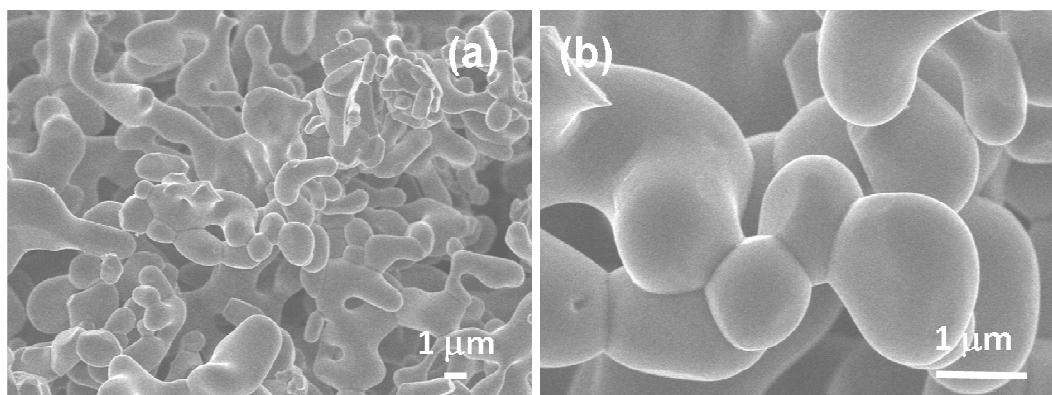


Fig. 7 SEM images of sample b with low (a) and high (b) magnification.

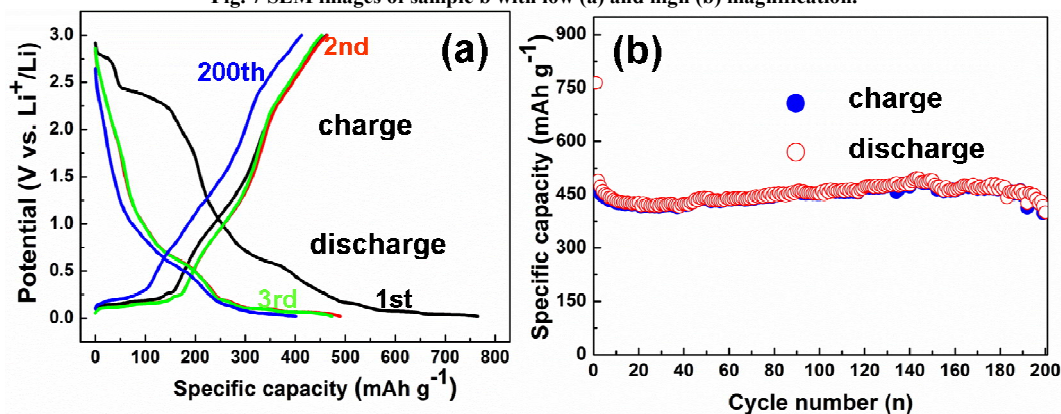


Fig. 8 The initial three and the 200th charge and discharge curves (a) and capacity retention (b) of $\text{CuV}_2\text{O}_6/\text{NG}$ electrode (sample b) at a specific current of 72 mA g^{-1} .

formation of stable SEI in cycling. Meanwhile, R_{ct} decreases along with the increase of cycle number, which is relevant to the electrochemical reconstruction that leads to the formation of a new integrated architecture in cycling, facilitating the electron transfer process. The EIS spectra of the $\text{CuV}_2\text{O}_6/\text{NG}$ electrode are in accordance with the SEM images as shown in Fig. 5.

Tab. 1 Electrode kinetic parameters obtained from equivalent circuit fitting of Nyquist plots for CuV_2O_6 electrodes.

| $\text{CuV}_2\text{O}_6/\text{NG}$ electrode | R_s/R_e (Ω) | R_{ct} (Ω) |
|--|------------------------|------------------------------|
| fresh | 11.01 | 51.31 |
| after 5 cycles | 15.72 | 40.92 |
| after 10 cycles | 7.02 | 31.44 |

According to XRD result, it can be deduced that the oriented growth of CuV_2O_6 was affected by the mol ratio of reaction materials. The morphology of sample b was contrastively studied. Fig. 7(a) is a low magnification SEM image of sample b, which shows a large number of micro-particles with mean size about $2 \mu\text{m}$. A high magnification SEM image of sample b is shown in Fig. 7(b), from which smaller particles with close combination can be observed. These small particles tend to grow into bigger ones, which suggests a possible Ostwald ripening growth mechanism.²¹ By comparing the fabrication condition of sample a and sample b, it can be deduced that excessive amount of V_2O_5 in the reaction material is beneficial for the oriented growth and size reduction of CuV_2O_6 .

The electrochemical performance of sample b was contrastively studied. Fig. 8(a) is the initial three and the 200th charge and

discharge curves of $\text{CuV}_2\text{O}_6/\text{NG}$ electrode (sample b) at a specific current of 72 mA g^{-1} . As seen, the profiles of charge and discharge curves are similar to those in Fig. 4(a), which suggest similar electrochemical reactions in charge/discharge process. Fig. 8(b) shows the capacity retention of the $\text{CuV}_2\text{O}_6/\text{NG}$ electrode. The initial discharge and charge capacity are 765 and 462 mAh g^{-1} , respectively. The irreversible capacity originates from lithium ions consumption owing to the irreversible phase transition.^{8,9} In the subsequent cycles, the charge and discharge capacity decrease slowly along with the increasing of cycle number and gradually reach stable values. After 200 cycles, the discharge and charge capacity maintain of 412 and 401 mAh g^{-1} , respectively. As seen, $\text{CuV}_2\text{O}_6/\text{NG}$ electrode obtained from sample a shows higher capacity and better cycle stability than the electrode obtained from sample b, which may be relevant to the specific morphology and size of CuV_2O_6 . Further studying the effects of morphology, size and impurity on the electrochemical performance of CuV_2O_6 are still under way.

In summary, the charge/discharge mechanism of CuV_2O_6 and the electrochemical performance of the $\text{CuV}_2\text{O}_6/\text{NG}$ as anode for Li-ion batteries were systemically studied. CuV_2O_6 undergoes structure variation in discharging that involves the first formation of LiV_2O_5 and $\text{Cu}_3\text{V}_2\text{O}_8$, the subsequent transition from $\text{Cu}_3\text{V}_2\text{O}_8$ to $\text{Li}_x\text{V}_2\text{O}_5$ and CuO , and the later reduction of CuO into Cu , which accompanies by an amorphization process. In the subsequent charging process, lithium ions are extracted from $\text{Li}_x\text{V}_2\text{O}_5$, and Cu is oxidized into Cu_2O . The superior

electrochemical performance of the CuV₂O₆/NG electrodes demonstrates great potential of CuV₂O₆ as anode for Li-ion batteries. Further more, maybe other vanadium based multiple oxides can be used as anode materials for Li-ion batteries.

5

Acknowledgement

We gratefully acknowledge the financial support from Natural Science Foundation of China (NSFC, 51302152, 51272128, and 51302153). Moreover, the authors are grateful to Dr. Jianlin Li at

10 Three Gorges University for his kind support to our research.

Notes and references

^a College of Materials and Chemical Engineering, China Three Gorges University, 8 Daxue Road, Yichang, Hubei 443002, China

^b Hubei Provincial Collaborative Innovation Center for New Energy Microgrid, China Three Gorges University +86 717 6397505. E-mail address: shibingni07@126.com. xlyang@ctgu.edu.cn

† Electronic Supplementary Information (ESI) available: [details of any supplementary information available should be included here]. See DOI: 10.1039/b000000x/

- 20 1 E. Antolini, *Solid State Ionics* 2004, **170**, 159-171.
- 2 A.K. Padhi, K.S. Nanjundaswamy, C. Masquelier, S. Okada and J.B. Goodenough, *J. Electrochem. Soc.* 1997, **144**, 1609-1613.
- 3 J. Lu, C.Y. Nan, Q. Peng and Y.D. Li, *J. Power Sources* 2012, **202**, 246-252.
- 25 4 D.H. Sim, X.H. Rui, J. Chen, H.T. Tan, T.M. Lim, R. Yazami, H.H. Hng and Q.Y. Yan, *RSC Adv.* 2012, **2**, 3630-3633.
- 5 T. Hillel and Y.E. Eli, *J. Power Sources* 2013, **229**, 112-116.
- 6 H.W. Liu and D.G. Tang, *Mater. Chem. Phys.* 2009, **114**, 656-659.
- 7 M. Morcrette, P. Martin, P. Rozier, H. Vezin, F. Chevallier, L. Laffont, P. Poizot and J. M. Tarascon, *Chem. Mater.* 2005, **17**, 418-426.
- 30 8 S.B. Ni, J.J. Ma, J.C. Zhang, X.L. Yang and L.L. Zhang, *J. Power Sources* 2015, **282**, 65-69.
- 9 H. Ma, S.Y. Zhang, W.Q. Ji, Z.L. Tao and J. Chen, *J. Am. Chem. Soc.* 2008, **130**, 5361-5367.
- 35 10 X.Y. Cao, J.G. Xie, H. Zhan and Y.H. Zhou, *Mater. Chem. Phys.* 2006, **98**, 71-75.
- 11 W. Hu, X.C. Du, Y.M. Wu and L.M. Wang, *J. Power Sources* 2013, **237**, 112-118.
- 12 G.Z. Yang, H. Cui, G.W. Yang and C.X. Wang, *ACS Nano*, 2014, **8**, 4474-4487.
- 40 13 S.B. Ni, X.H. Lv, T. Li, X.L. Yang and L.L. Zhang, *Electrochim. Acta* 2013, **109**, 419-425.
- 14 S.B. Ni, J.J. Ma, J.C. Zhang, X.L. Yang and L.L. Zhang, *Electrochim. Acta* 2015, **153**, 546-551.
- 45 15 S.B. Ni, T. Li, X.H. Lv, X.L. Yang and L.L. Zhang, *Electrochim. Acta* 2013, **91**, 267-274.
- 16 C. Wang, D.L. Wang, Q.M. Wang and H.J. Chen, *J. Power Sources* 2010, **195**, 7432-7437.
- 17 S.B. Ni, X.H. Lv, T. Li, X.L. Yang, L.L. Zhang and Y. Ren, *Electrochim. Acta* 2013, **96**, 253-260.
- 50 18 S.B. Ni, X.H. Lv, J.J. Ma, X.L. Yang and L.L. Zhang, *J. Power Sources* 2014, **270**, 564-568.
- 19 T.F. Yi, A.K. Fang, Y. Xie, Y.R. Zhu and S.Y. Yang, *ACS Appl. Mater. Interfaces* 2014, **6**, 20205-20213.
- 55 20 Y.J. Zhu and C.S. Wang, *J. Phys. Chem. C* 2011, **115**, 823-832.
- 21 B.P. Jia and L. Gao, *J. Cryst. Growth* 2007, **303**, 616-621.